Received: 5 April 2024 | Revised: 5 June 2024 | Accepted: 12 June 2024

DOI: 10.1002/bit.28783

ARTICLE

BIOTECHNOLOGY AND BIOENGINEERING WILEY

Tailoring silk fibroin fibrous architecture by a high-yield electrospinning method for fast wound healing possibilities

Jia-Chen Zhu[1] | Hui Wang[2] | Chen-Xing Wu[2] | Ke-Qin Zhang[2] | Hua Ye[1,3]

[1]Oxford Suzhou Centre for Advanced Research, University of Oxford, Suzhou, Jiangsu, China

[2]National Engineering Laboratory for Modern Silk, College of Textile and Clothing Engineering, Soochow University, Suzhou, China

[3]Institute of Biomedical Engineering, Department of Engineering Science, University of Oxford, Oxford, UK

Correspondence

Hui Wang, National Engineering Laboratory for Modern Silk, College of Textile and Clothing Engineering, Soochow University, Suzhou, Jiangsu, China.
Email: whui@suda.edu.cn

Ke-Qin Zhang, National Engineering Laboratory for Modern Silk, College of Textile and Clothing Engineering, Soochow University, Suzhou, Jiangsu, China.
Email: kqzhang@suda.edu.cn

Hua Ye, Institute of Biomedical Engineering, Department of Engineering Science, University of Oxford, Oxford, UK.
Email: hua.ye@eng.ox.ac.uk

Funding information

Royal Society, Grant/Award Number: IEC \NSFC\181408; National Natural Science Foundation of China, Grant/Award Number: 51911530207; Natural Science Foundation of Jiangsu Province of China, Grant/Award Number: BK20211317; China National Textile and Apparel Council Key Laboratory for Silk Functional Materials and Technology; Priority Academic Program Development of Jiangsu Higher Education Institutions

Abstract

In this study, a novel array electrospinning collector was devised to generate two distinct regenerated silk fibroin (SF) fibrous membranes: ordered and disordered. Leveraging electrostatic forces during the electrospinning process allowed precise control over the orientation of SF fiber, resulting in the creation of membranes comprising both aligned and randomly arranged fiber layers. This innovative approach resulted in the development of large-area membranes featuring exceptional stability due to their alternating patterned structure, achievable through expansion using the collector, and improving the aligned fiber membrane mechanical properties. The study delved into exploring the potential of these membranes in augmenting wound healing efficiency. Conducting in vitro toxicity assays with adipose tissue-derived mesenchymal stem cells (AD-MSCs) and normal human dermal fibroblasts (NHDFs) confirmed the biocompatibility of the SF membranes. We use dual perspectives on exploring the effects of different conditioned mediums produced by cells and structural cues of materials on NHDFs migration. The nanofibers providing the microenvironment can directly guide NHDFs migration and also affect the AD-MSCs and NHDFs paracrine effects, which can improve the chemotaxis of NHDFs migration. The ordered membrane, in particular, exhibited pronounced effectiveness in guiding directional cell migration. This research underscores the revelation that customizable microenvironments facilitated by SF membranes optimize the paracrine products of mesenchymal stem cells and offer valuable physical cues, presenting novel prospects for enhancing wound healing efficiency.

KEYWORDS

array electrospinning collector, cell migration, physical cues, secretion products, silk fibroin, wound healing

1 | INTRODUCTION

The process of wound healing is intricate and multiphased, involving hemostasis, inflammation, proliferation, and maturation. However, it may halt at the inflammation or proliferation stage, transforming a normal wound into a chronic one, which can cause discomfort to patients. Wound healing efficiency is worth paying attention to in preventing complications such as amputations in diabetic foot ulcer patients and halting the progression of acute wounds into chronic ones (Sharifi et al., 2020; Zhang et al., 2022). During the inflammation and proliferation stages, fibroblasts are recruited to the wound site guided by factors produced by macrophages and other immune cells and physical cues from the extracellular matrix (ECM). Hence, the migration of fibroblasts into the wound is considered an important factor in ensuring a smooth wound healing process to improve wound healing efficiency, particularly the process of transition from inflammation to the proliferation stage.

The complex fibrous network environment presented by the in vivo ECM can support the wound healing process and dynamically regulate cellular physiological behavior by transmitting biochemical signal cues (Collins et al., 2021). Micro/nano fibrous membranes are gaining increasing attention as wound healing materials due to their high similarity with in vivo ECM (Ge et al., 2020; Huang et al., 2017). In in vitro wound healing models, leading-edge cells responsible for tissue repair often exhibit random movement due to factors such as cell density (Shellard & Mayor, 2020). While cells possess the ability to translate the topographical cues presented by micro/nano fibrous membranes, leading to alterations in their shape and movement direction, ultimately recruiting cells to the cell gap (Memic et al., 2019). Numerous studies involving different cell types have demonstrated that both fiber diameter and alignment positively influence cell migration (Gholipourmalekabadi et al., 2020). For example, fibrous silk fibroin (SF) scaffolds with aligned features have proven effective in expediting cell migration toward wounds, facilitating processes like neovascularization, tissue infiltration, and the formation of new skin layers (Gao et al., 2021). However, there are too many studies focusing solely on the physical cues guiding migration. It is essential to observe from multiple perspectives, as micro/nano fibers themselves also influence paracrine signaling, substituting immunomodulatory cytokines to render cells chemotactic. For example, creating a specialized microenvironment with micro/nano fibrous membranes effectively optimizes mesenchymal stem cells (MSCs) paracrine signals, fostering chondrogenesis, migration, proliferation, and anti-inflammatory responses (Kadunc Polajnar et al., 2023). The mechanical cues from distinct fiber orientations activate a variety of focal adhesion kinase - extracellular signal-regulated kinase signaling pathways, shaping paracrine effects (Xie et al., 2022).

Among the micro/nano fiber fabrication technologies, electrospinning stands out as a cost-effective and straightforward method that enables the creation of membranes composed of micro- and nano-fibers to imitate the native dermal ECM (Zhang et al., 2021). Its potential applications in wound healing therapy are substantial, encompassing drug delivery (e.g., growth factors, anti-inflammatory drugs, live cells) (Ji et al., 2020; Mousavi et al., 2021), the promotion of cell secretion (Imaichi-Kobayashi et al., 2023), and the guidance of cell behavior (Li et al., 2017). Among the various polymer options, numerous studies have demonstrated the superiority of SF in various forms as therapeutic wound dressings that facilitate the healing process (Wang et al., 2023), including hydrogels, sponges, films, electrospun nanofiber membranes, and hydrocolloid dressings (Jiao et al., 2023). The collector architecture and the control over the electrostatic field can effectively affect the fiber arrangement, so as to obtain the aligned micro/nano fibrous membranes (Robinson et al., 2021). However, challenges arise, particularly when producing aligned electrospun fibers through selecting specific collectors like a rotating cylindrical roller or parallel electrodes. The aligned micro/nano fibrous membranes produced by traditional electrospinning methods are usually relatively thin, as well as anisotropic and sparse interconnection together, making the fibrous membranes mechanically unstable. Therefore, the aligned fibrous membrane is easily destroyed by external forces under experimental, surgical, and wet physiological environment conditions, which greatly limits its application in vitro and in vivo biomedical fields (Navaneethan et al., 2021; Yao et al., 2020).

In this study, a new type of array electrospinning collector has been developed that can not only accurately control the fiber orientation distribution but also realize the simultaneous and efficient preparation of ordered and disordered SF fiber membranes, as shown in Figure 1a. The array electrospinning collector in the electrospinning process provided a suitable electric field for the deposition of each aligned and randomly arranged SF fiber layer and realized the efficient fabrication of patterned SF membrane material arranged in ordered/disordered array arrangement. Compared with the traditional single-ordered fibrous membrane, the patterned membrane exhibited improved mechanical properties and maintained highly aligned fiber orientation during area expansion. The patterned membrane was divided into two samples according to fiber orientations, the ordered region membranes (SF-Fr-O) and the disordered region membranes (SF-Fr-D) for further research (Figure 1b). In addition, the flat SF membrane prepared by direct curing of regenerated SF solution was referred to as silk fibroin flat (SF-Ft) as a reference sample. Here, all three materials (SF-Fr-O, SF-Fr-D, and SF-Ft) were designated as growth platforms for both normal human dermal fibroblasts (NHDFs) and adipose tissue-derived mesenchymal stem cells (AD-MSCs). We use dual perspectives on exploring the effects of different conditioned mediums (CMs) produced by cells and structural cues of materials on NHDFs migration. When evaluating the secreted products of AD-MSCs and NHDFs in the form of CMs, the primary emphasis is on assessing paracrine effects. Also, the physical structural cues of materials on NHDFs migration are assessed through changes in cell morphology, orientation, and migration speeds. The ordered and disordered nanofibers providing the microenvironment can directly guide NHDFs migration and also affect the AD-MSCs and NHDFs paracrine effects, which can improve the chemotaxis of NHDFs migration. The research takes a new approach by exploring the influence of CMs generated by cells in response to their microenvironment and the

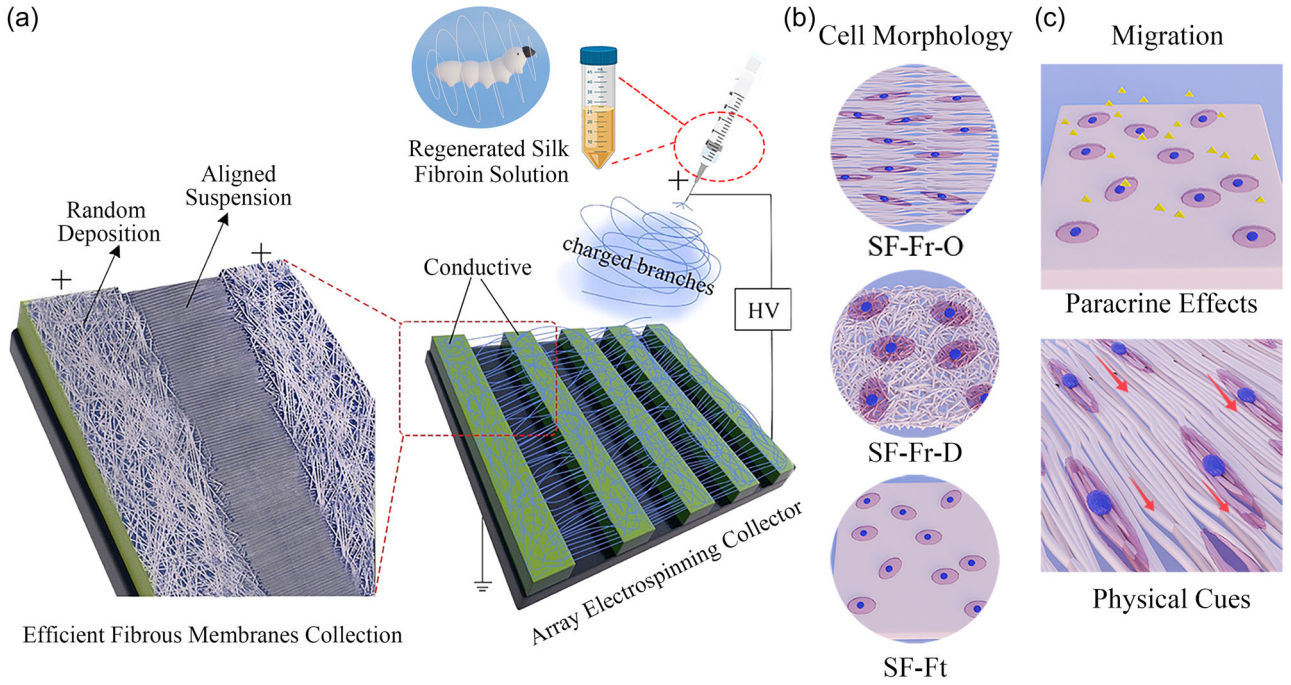

FIGURE 1 (a) Schematic diagram illustrating the array electrospinning collecting system used for highly efficient membrane collection. This system enables the simultaneous collection of both randomly and aligned fiber membranes during a single electrospinning process. The fibers are suspended sequentially across the inclined gap while also being randomly deposited on the gap. The electrospinning solution used was extracted from natural *Bombyx mori* silk. (b) Morphology of adipose tissue-derived mesenchymal stem cells or normal human dermal fibroblasts grown on the SF-Fr-O, SF-Fr-D, and SF-Ft. (c) Cell migration promotion effects were assessed by the secretion products, in the form of conditioned mediums, and physical cues.

inherent cues provided by the materials themselves, presenting new ideas for enhancing wound healing efficiency.

2 | MATERIALS AND METHODS

2.1 | Fabrication of SF materials

Raw silk fibers (Huzhou Zhesi Second Factory Co., Ltd.) underwent a degumming process involving three cycles in a 0.5 g/L Na_2CO_3 solution (Sinopharm Chemical Reagent Co., Ltd.) at 100°C for 30 min, with regular stirring. Subsequently, the entire mass was thoroughly rinsed with warm deionized water to eliminate sericin, a glue-like substance, and then dried in an oven at 30°C overnight. The degummed silk fibers were dissolved in a prewarmed 9.3 M LiBr solution (Sigma-Aldrich) at 60°C for 2 h. The resulting fibroin solution underwent dialysis using a cellulose membrane-based dialysis cassette (Mv 3.5 kDa) against deionized water for a duration of 3 days, with water changes performed every 6 h to remove LiBr. Following dialysis, the regenerated SF solution was subjected to centrifugation at 5°C and 9000 rpm for 20 min. Finally, the regenerated SF solution was freeze-dried for subsequent preparation into an electrospinning solution.

The electrospun solution is a ternary system of 14 wt.% freeze-dried regenerated SF and 0.05 wt.% polyethylene oxide (PEO, Mv:1,000,000, Sigma-Aldrich) in formic acid (98%, Sigma-Aldrich). PEO is a synthetic polymer that has been widely utilized in electrospinning for biomedical applications. This is due to its nontoxicity and its ability to dissolve in both aqueous solutions and organic solvents. Here, we have chosen PEO as a supporting material to enhance the electrospinning process of SF. This solution was magnetically stirred for 24 h at 4°C. The mixed solution was loaded into a syringe with a 0.26 mm needle. The flow rate was set at 0.5 mL/h, and an applied voltage of 12 kV was used with a 15 cm collecting distance.

For the 14 wt.% regenerated SF dissolved in formic acid to create flat membranes at the same concentration as the electrospinning solution but without PEO, each 5 mL of the solution was dried in a 9 cm glass dish at 30°C for 24 h. All three types of SF materials were immersed in 80% ethanol for 30 min to induce crystallization and insolubility. Subsequently, they were immersed in deionized water to remove PEO and ethanol.

2.2 | Characterization of SF materials

The microstructure of both fibrous membranes and flat membranes was observed using a field scanning electron microscope (SEM; S4800) after the samples had been sputtered with gold for 120 s. Image analysis was performed using ImageJ software to determine the mean fiber diameter, diameter distribution, and fiber orientation.

To calculate the mean fiber diameter, 500 fibers were randomly selected from 10 SEM images ($n = 10$). For the analysis of fiber orientation distribution, fast Fourier transforms (FFTs) were used. FFTs transform the signal from the time domain to the frequency domain. The location was displayed in polar coordinates, the angle was expressed in degrees, and the radius was expressed in pixels. Therefore, the orientation distribution sums the total intensity for each angle radially (Taylor et al., 2013).

The chemical structure of the prepared samples was analyzed using Fourier transform infrared spectroscopy with the total reflection method (FTIR-ATR, Nicolet-5700). FTIR-ATR spectra were obtained in the wavenumber range from 2500 cm^{-1} to 600 cm^{-1} during 32 scans, with 4 cm^{-1} resolutions. FTIR-ATR was used further to analyze the change of SF secondary structure.

The mechanical properties of the SF membranes were investigated with a tensile tester (ENGYI). The fibers were cut in strips with a size of $30 \times 10\ mm^2$. The tests were conducted with a crosshead speed of 10 mm/min at room temperature and 60% humidity. The ultimate tensile strength and elongation at break were calculated from the stress–strain curve.

2.3 | AD-MSCs and NHDFs culture

AD-MSCs and NHDFs were purchased from PromoCell GmbH Inc. AD-MSCs and NHDFs were respectively expanded in MSC growth medium 2 (PromoCell) and fibroblast growth medium 2 (PromoCell) in the incubator, which had an atmosphere of 5% CO_2 at 37°C. The medium was changed every 48 h. When the cells covered 80%–90% of the bottom of the flask, they were digested with 0.05% trypsin-EDTA (Invitrogen) and collected for passage. AD-MSCs and NHDFs were used in passage 8 and passage 10 for further experiments, respectively.

2.4 | Toxicity assay

Toxicity assay was determined by measuring the metabolic activity and proliferation of AD-MSC and NHDFs after exposure to the SF materials immersed medium. SF materials were cut to fit 24-well plates and immersed in MSC growth medium 2 (PromoCell) supplemented with 1% penicillin-streptomycin (Invitrogen). The collection of the immersed medium was maintained by adding fresh medium every 48 h at the ratio of a sample with 1 mL medium. The same culture condition without materials in the medium and fresh MSC growth medium were used as controls. The AD-MSCs and NHDFs were seeded in 24-well plates at a density of 8×10^3 cells per well. After 24 h of proliferation and attachment, the cells were rinsed twice with 1 mL of Dulbecco's phosphate-buffered saline (D-PBS) and then exposed to 1 mL of the SF materials immersed medium per well.

After exposure to the extract medium, day 0 was designated as the starting point. Before the assay, the cells were rinsed twice with D-PBS. Absorbance measurements were taken at 450 nm using a microplate reader (Spark Control, Tecan) via the Cell Counting Kit-8 (CCK8, Dojindo) assay on days 1, 2, 4, 6, and 8. The OD450 values of different groups were normalized against the blank samples at their respective time points.

2.5 | Tunable CM effects on wound healing

In vitro wound healing assessments were conducted using a wound test. AD-MSCs and NHDFs were cultured on three different surfaces to collect CM at the density of 1.2×10^4 cells per 24-well. The three surfaces were SF-Fr-D, SF-Fr-O, and SF-Ft. The materials were cut into 24-well sizes and washed twice with D-PBS, each for 10 min as pretreatment. After 24 h of cell adhesion and proliferation, the medium was replaced with serum-free low-glucose Dulbecco's modified eagle medium (LG-DMEM, Sigma-Aldrich) supplemented with 1% penicillin-streptomycin (Invitrogen). CM was collected 24 h later, and the collected CM was centrifuged at 1500 rpm for 10 min to remove dead cells and cellular debris. It was then stored at 4°C with a tight seal for not more than 4 h before use.

To ensure that all CM from different surfaces and cells contained the same protein concentration, the protein content of CM was determined using the Bicinchoninic Acid assay (BCA, Sigma-Aldrich). Subsequently, the protein concentration of CM was diluted to 85, 250, and 450 μg/mL using serum-free LG-DMEM.

Here, a gap was created using culture inserts (ibidi) that were affixed to the plates, serving as templates to guide cell attachment. P11 NHDFs were seeded onto the inserts at the intensity of 1×10^5 cells with 1.5 mL of medium per well to form a monolayer. After 24 h of attachment, the inserts were carefully removed, creating a 500 μm gap in the center, surrounded by a 1000-μm-wide square pattern. The cell patterns were subsequently washed twice with D-PBS before adding the diluted CM. The time of CM addition was designated as hour 0. Cell migration was observed over a 72-h period using a bright-field microscope (X53, Olympus), and images were captured at each time point. Image analysis was performed using the ImageJ software to measure the gap area. The wound closure percentage was calculated as the ratio of the reduced gap area compared to the initial gap area at hour 0.

2.6 | Physical cues for fast wound healing

Fluorescence and SEM methods have been used to examine the morphology of AD-MSCs and NHDFs on SF materials. Before cell seeding, the materials were washed with D-PBS twice each for 10 min. Cells were then seeded onto the surfaces of the samples through natural sedimentation at a density of 8×10^3 cells per 24-well. It was then placed in a 5% CO_2 atmosphere and incubated in a 37°C incubator.

The 10 μg/mL fluorescein diacetate (FDA; Invitrogen) was used as the viability probe to observe live cells. FDA becomes fluorescent when activated by intracellular esterase in viable cells. After 5 min

incubation of FDA, cell morphology was observed with a laser scanning confocal microscope (Olympus, FV3000).

For SEM analysis, the samples underwent several steps. Initially, they were washed with D-PBS and then fixed overnight in a 2.5% glutaraldehyde solution at 4°C. Subsequently, the samples were sequentially dehydrated using increasing concentrations of ethanol (30%, 40%, 50%, 70%, 80%, 90%, 95%, and 100%). Between each ethanol treatment, the samples were rinsed with D-PBS for 15 min to remove any residual glutaraldehyde. Following the dehydration process, the samples were subjected to drying in a freeze dryer for 4 h and then coated with a thin layer of gold using a sputtering process lasting 120 s. Finally, the prepared samples were examined using a field SEM (S4800) at an operating voltage of 20 kV, with magnifications ranging between 800 and 2000 times.

Additionally, this is aimed at investigating cell-material interactions and assessing the impact of topographical cues. Long-term tracking of NHDFs P8 on SF material surfaces was conducted using a laser scanning confocal microscope (FV3000, Olympus) equipped with a ×20 dry objective. When NHDFs coverage reached approximately 80% of the flask bottom, NHDFs were prepared for membrane staining using 4 μM PKH26 (Sigma-Aldrich), following the protocol recommended by Sigma.

Here, the steps were carried out as the protocol sigma suggested. NHDFs were resuspended in the serum-free fibroblast growth medium 2 (Promocell) supplied with 1% penicillin-streptomycin (Invitrogen). The NHDFs were seeded on the surfaces of SF-Fr-D, SF-Fr-O, SF-Ft, and glass-bottom plates at the density of 5×10^5 cells/mL. After 24 h of attachment, the materials were flipped over and placed into a glass-bottom plate. Cells were maintained in the medium in a 37°C, 5% CO_2 incubator chamber, which was attached to the confocal. A laser detected the dyes at an excitation wavelength of 450 nm. Using the map mode, each sample was z-scanned to capture the entire fluorescence signal every 30 min, lasting for 24 h to track cell migration. The tracking point of NHDFs was automatically identified from the center of cells at each time point using an ImageJ plugin called TrackMate (http://fiji.sc/TrackMate) (Loesel et al., 2023). Trajectories were defined using coordinates to describe migration distance and direction, with the initial positions calibrated as "0,0." The Chemotaxis and Migration Tool software (ibidi) was used to measure cell directionality, Euclidean distance, accumulated distance, and velocity.

2.7 | Statistical analysis

Three distinct experiments were carried out independently to assess both toxicity and cell migration. In each experiment, there were three replicate samples for every condition, resulting in a total of three experiments, each with its own set of replicates ($n = 3$). For the toxicity experiment, the Tukey test was subsequently employed to make pairwise comparisons between the two groups. CM-migration analysis was conducted using multifactorial analysis of variance (ANOVA) procedures, facilitated by SPSS software. In cases where significant main effects were observed, post hoc Tukey pairwise comparison procedures were employed for further analysis. Notably, significant interaction effects were also plotted. The results of this study are presented in the form of mean ± standard deviation, with statistical significance indicated by $p < 0.05$. This rigorous methodology enhances the reliability and strength of the collected data.

3 | RESULTS AND DISCUSSION

3.1 | Characterization of the SF materials' physicochemical properties

A 3D-printed static array electrospinning collector has been developed to guide fiber deposition in two ways. The photo shows alternating patterned membranes on the collector, with dimensions of 13 cm width and 19 cm length (Figure 2a). Large areas of ordered fibrous membranes can be efficiently gathered while maintaining their integrity over time by inserting the disordered regions. During the deposition process, charged SF branches are suspended sequentially across the inclined gap to create ordered fibers (SF-Fr-O). In contrast, other branches deposited on the gaps appear in a disordered arrangement, forming disordered fibers (SF-Fr-D). Both SF-Fr-D and SF-Fr-O exhibited similar membrane thickness and porosity (Figure 2b). There was always a difference between the SF-Fr-D and SF-Fr-O in fiber diameter and diameter distribution (Figure 2c). This could be attributed to the reduced electric field force between the gaps, leading to less stretching of the fibers. SEM images were processed using FFT to represent the distribution of fiber orientation (Figure 2d) (Brandley et al., 2018). In terms of fiber orientation, both the qualitative morphology and quantitative data clearly demonstrated differences between the two types of fibers. The fiber orientation of SF-Fr-D after electrospinning was random and isotropic, while SF-Fr-O fibers were highly oriented, influenced by the collector.

In most cases, aligned fibers are collected using dynamic collectors, such as a rotating cage or narrow plate (Robinson et al., 2021). A thin membrane is produced efficiently by the rotating cage due to the limited control over the electric field; the degree of alignment is affected by extended processing times and thicker electrospun fibers (In Kim & Kim, 2018). Although magnetic fields (Raymond Kevin Tindell & Julianne, 2023) and auxiliary electrodes (Oroujzadeh et al., 2024) have been applied to produce aligned membranes, the membrane area is insufficient, and the elongation at break is weaker compared to the normal electrospun membrane. The array electrospinning collector will overcome these limitations. It can improve the mechanical properties by inserting disordered regions in the whole membrane. And getting larger areas by alternating regions, which can produce two distinct types of fibers in a single electrospinning process.

The insoluble treatment transforms water-soluble SF membranes into insoluble ones, enhancing their application in wound healing. This treatment is a method to induce a conformational transition in SF from α-helices or random coils into a β-sheet structure and increase crystallinity by adding low dielectric constant organic

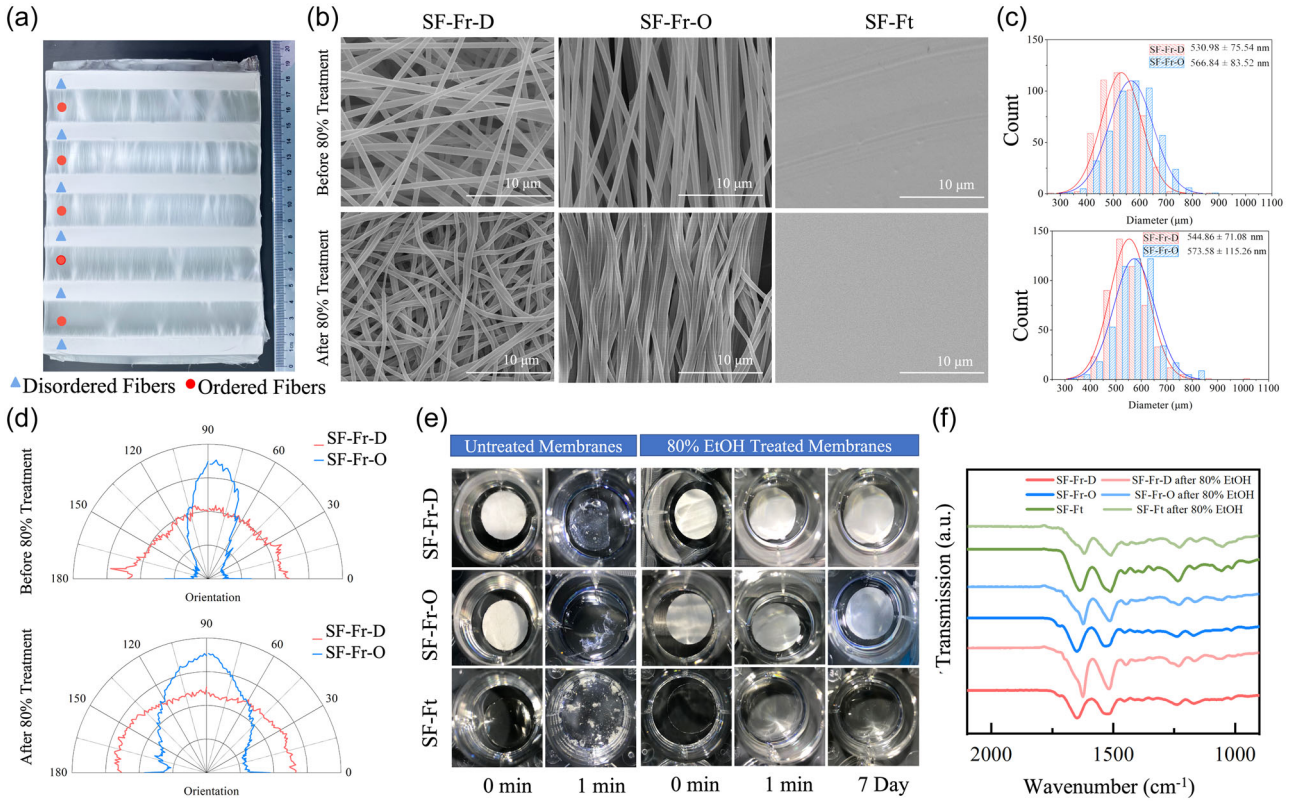

FIGURE 2 Collecting alternating patterned membranes and their insoluble treatment. (a) The photo of alternating patterned membranes on the array electrospinning collector, including ordered and disordered membranes. (b) Scanning electron microscope (SEM) images. (c) Fiber diameter distribution. (d) Fiber orientations of SF-Fr-O and SF-Fr-D before and after the 80% ethanol treatment. SEM images were processed with Fast Fourier Transform, which represents the orientation of fibers. (e) Photos illustrating insoluble SF-Fr-D, SF-Fr-O, and SF-Ft in Dulbecco's phosphate-buffered saline after 80% ethanol treatment. (f) Fourier Transform Infrared Spectroscopy with the total reflection method diagram of silk fibroin materials both before and after 80% ethanol treatment. The mean and distribution of fiber diameter were measured by selecting 500 fibers randomly from 10 images obtained from three independent experiments and presented as the mean ± standard deviation, with $n = 3$ replicates for each measurement.

solvents such as methanol, ethanol, or dioxane (Nogueira et al., 2010). Here, we choose 80% ethanol treatment. The SEM images after the water-insoluble treatment revealed that the fibers became twisted and adhered to each other, resulting in decreased porosity (Figure 2b). However, the treatment did not significantly affect the fiber diameter, distribution, and orientation (Figure 2c,d). It increases the crystallinity and reduces the water solubility of the treated samples, as shown in Figure 2e. Following insoluble treatment, the three types of SF membranes retained their membrane integrity and remained insoluble in D-PBS for a period of up to 7 days. In contrast, the three untreated SF membranes rapidly disintegrated upon exposure to D-PBS, dissolving in the solution and disappearing within 1 min. It signifies that the insoluble treatment is an irreversible transformation process. The FTIR-ATR spectra of SF-Fr-D, SF-Fr-O, and SF-Ft before and after ethanol treatment are displayed in Figure 2f. SF-Fr-O, SF-Fr-D, and SF-Ft, before ethanol treatment, exhibited absorption bands at 1530 cm^{-1} (amide II) and 1656 cm^{-1} (amide I), indicative of the typical random coil. After ethanol treatment, new absorption bands appeared at 1623 cm^{-1}, associated with amide I, as well as at 1527 cm^{-1} for amide II. These results indicate that the secondary structure of SF-Fr-D, SF-Fr-O, and SF-Ft underwent a conformational transition from random coils to a β-sheet structure. This transformation in the secondary structure and changes in crystallinity are responsible for the insoluble properties observed. During the ethanol treatment process, SF undergoes a conformational transition from α-helices or random coils to a β-sheet structure. This treatment helps strike a balance between structural changes and insolubility, making the material suitable for wound healing applications.

The stress–strain curves of SF-Fr-D, SF-Fr-O, and alternating pattern membranes are shown in Supporting Information S1: Figure S1. The results show that the tensile strength of SF-Fr-D is low, but there can be a certain degree of tensile deformation. However, the tensile strength of SF-Fr-O in the dominant direction is significantly higher than that of SF-Fr-D, but the elongation is very low, only 5.1%, showing brittle characteristics. Although the tensile strength of the patterned fibrous membrane is slightly lower than that of SF-Fr-O (about 2.4 MPa), its elongation at break is significantly increased, from 5.1% to 31.2%. By inserting the disordered membranes, the aligned fibrous membrane avoided

abrupt failure, resulting in an ordered fibrous membrane with a larger size and better integrity.

3.2 | Toxicity assay of the SF materials

The toxicity test, which is an indirect evaluation, aimed to assess whether the materials would inhibit cell growth. This was done by culturing AD-MSCs and NHDFs in a medium that had been exposed to the materials. The CCK8 mixture was directly added to the 24-well plate where the AD-MSCs and NHDFs were adhered to the material surface. The optical density of the mixture was measured at 450 nm (OD450) using a microplate reader after 4 h of incubation on days 1, 2, 4, 6, and 8. The OD450 values represented the in situ metabolic activity and proliferation of AD-MSCs and NHDFs after being exposed to the material extracts. The OD450 values of the samples were corrected for background values by subtracting the OD450 values of the blank. The observed growth curves show that AD-MSCs experienced a rapid increase in metabolic activity from day 2 to day 4 (Figure 3a), while NHDFs exhibited their highest growth rates between day 4 and day 6 (Figure 3b). This disparity in growth rates indicates differences in the metabolism and proliferation behaviors of these two cell types, with AD-MSCs displaying a more robust growth profile compared to NHDFs.

Additionally, the analysis of variance between material groups for each cell type did not reveal significant differences. This suggests that SF-Fr-O, SF-Fr-D, and SF-Ft materials did not have any adverse effects on the proliferation of AD-MSCs or NHDFs when compared to the blank groups. Importantly, the material extracts did not significantly inhibit the proliferation of AD-MSCs and NHDFs. These results indicate that there were no statistically significant differences in cell viability between the material groups (fibrous membranes and flat membranes) and the control groups (without materials and fresh medium) for both Ad-MSCs and NHDFs. Therefore, it can be concluded that the prepared SF-Fr-O and SF-Fr-D did not exhibit a significant toxic effect on the viability of these cell types. The entire protocol, including SF extraction and electrospun solution formulation, is deemed nontoxic, and SF materials are considered to have good biocompatibility, with no evidence of chemical residue or SF precipitation.

3.3 | Tunable CM effects on wound healing

CM denotes the phenomenon where, as cells are cultured in a medium over a period, the medium accumulates bioactive molecules and extracellular vesicles that are secreted by these cells. CM serves as a medium of cellular communication, housing a diverse array of bioactive compounds generated by the cells themselves, including growth factors, cytokines, hormones, proteins, and more. These bioactive molecules can elicit various effects, including the promotion of cell proliferation, facilitation of cell migration, and induction of cell differentiation (Maarof et al., 2018). Recent research has highlighted that different structural configurations can stimulate cell–matrix interactions and activate mechanical transduction signal cascades, ultimately influencing the secretory profile of cells (Lian et al., 2021). Notably, transforming growth factor β1 and bone morphogenetic protein 2, both of which promote cell migration and chondrogenesis, show comparable upregulation when cells secrete on fibrous surfaces (Kadir et al., 2021; Xia et al., 2017). In addition, aligned fibers have been found to be particularly effective in enhancing chondrogenesis due to the elevated levels of Interleukin-8 (Dahbour et al., 2017).

A scratch test was conducted to assess the migratory potential of CM generated from different sources, including SF-Fr-D, SF-Fr-O, and SF-Ft. The results were evaluated using varying CM concentrations (450, 250, and 85 μg/mL) and different cell types (AD-MSC and NHDF) to study the migration of NHDFs. This tunable paracrine effect, modulated by electrospun membranes, holds significant promise for expediting wound healing. In addition, surfaces composed of SF-Ft have been designed to show physical differences compared to fibrous membranes. The data were analyzed by multifactorial analysis of variance (ANOVA). Independent variables included cell, material,

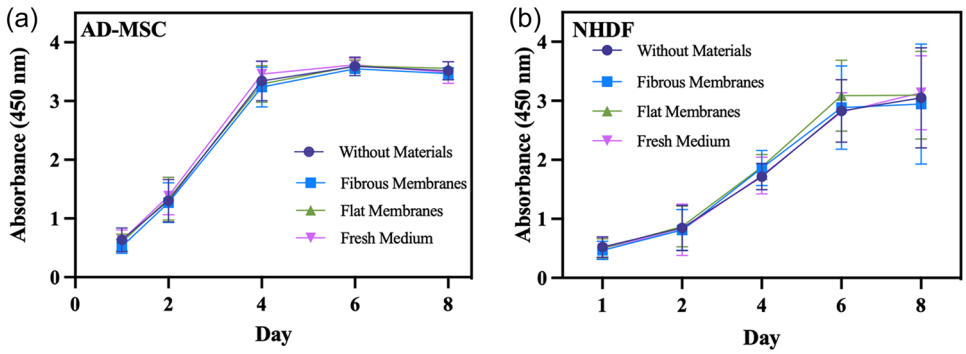

FIGURE 3 Metabolic viability assay (Cell Counting Kit-8) of adipose tissue-derived mesenchymal stem cells (AD-MSCs) (a) and normal human dermal fibroblasts (NHDFs) cells (b) on the prepared fibrous membranes (SF-Fr-O and SF-Fr-D) and flat membranes (SF-Ft) at the desired time point at 1, 2, 4, 6, and 8 days of culture. The control groups include those without materials and fresh medium. The data underwent analysis through ANOVA, and the results represent the average from three independent experiments, with values averaged by replicates ($n = 3$). The data are presented as the mean ± standard deviation with a 95% confidence interval, and statistical significance was determined as $p < 0.05$.

concentration, and hour. Grouping information using the Tukey pairwise comparisons method and 95% confidence. Photographs were taken at 4, 7, 11, 17, 23, 29, 38, 42, 48, 60, 72 h and beginning on the day of wounding. Time-to-closure was defined as the number of hours for complete cover of the gap. The wound area was measured by calculating the area of the gap by the software ImageJ. Percentage wound closure was calculated by the following formula:

$$\text{Wound Closure Percentage\%} = \frac{A_{t=0h} - A_{t=\Delta h}}{A_{t=0h}} \times 100\%$$

where A_t = 0 h is the area of the wound measured immediately after scratching (t = 0 h) and A_t = Δh is the area of the wound measured h hours after the scratch is performed.

The CM produced by cells cultured on different material surfaces exhibited varying protein concentration levels as determined by the BCA assay (Figure 4a). In comparison to SF-Ft, fibrous surfaces including SF-Fr-O and SF-Fr-D resulted in higher protein concentrations in both MSCs and NHDFs' CM. Among these fibrous surfaces, MSCs cultured on SF-Fr-O exhibited the highest protein secretion concentration, with significant differences with the CM from MSCs on SF-Ft. These findings suggest that a fibrous surface can stimulate cells to secrete higher protein concentrations. This implies that the influence of material surfaces on cell behavior may differ from traditional culture conditions.

When compared to Dulbecco's modified eagle medium, the CM contained factors that promote cell migration (Figure 4b). These results provide robust evidence supporting the idea that the topological structures of SF indeed influence cellular paracrine signaling to influence cell chemotaxis. Both cell type and material independently played a substantial role in the observed disparities in wound closure percentage (Supporting Information S1: Table S1). MSCs derived CM is consistently regarded as a favorable candidate for paracrine effects on wound healing. AD-MSCs CM consistently exhibited a more pronounced promotion of NHDFs migration compared to NHDFs CM, resulting in enhanced wound closure percentage (Supporting Information S1: Figure S2). The distinct microenvironments created by different materials result in the generation of CM containing varying contents when cells are cultured within them. These CM, with their differing compositions, significantly influence wound closure percentage, especially the material and cell types that play an important role. The significant interactions between cell type and material, evident whenever variations in wound closure percentage were observed, indicate that the microenvironments created by these materials are unique and different cell types exhibit diverse requirements (Figure 4c). The inconsistency in the effects of NHDFs CM and AD-MSCs CM, derived from different materials, became apparent when specific material sources were

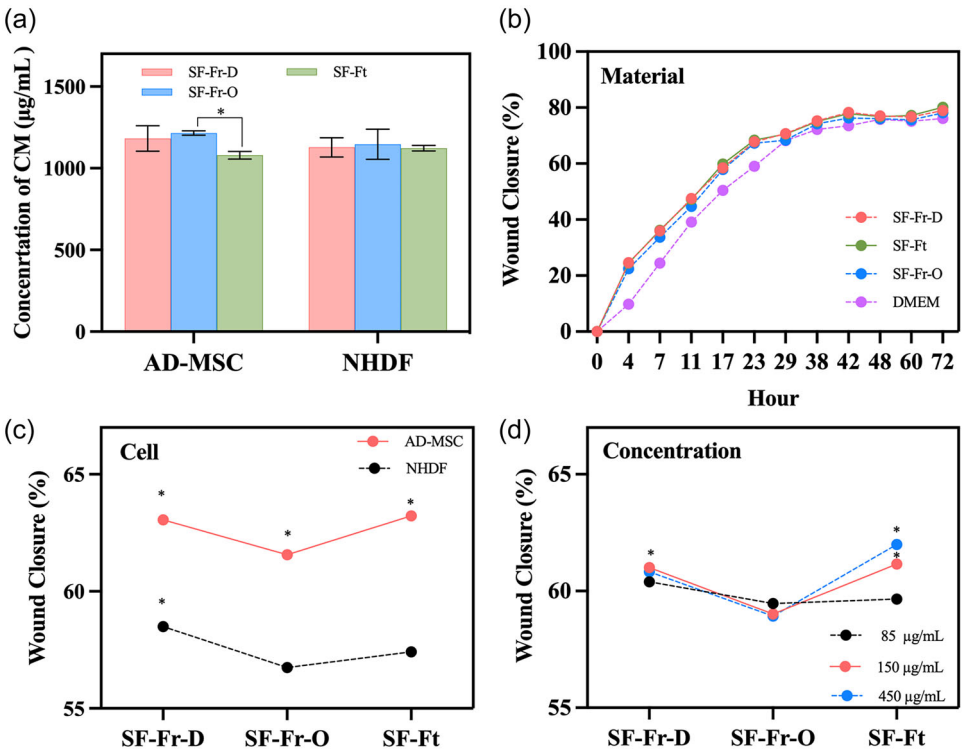

FIGURE 4 The conditioned mediums (CMs) from both adipose tissue-derived mesenchymal stem cells (AD-MSCs) and normal human dermal fibroblasts (NHDFs) on silk fibroin (SF) materials and their effects on NHDFs migration. (a) Protein concentration of the CMs from AD-MSCs and NHDF on SF materials. NHDFs migration data were analyzed by a two-way interaction plot employing ANOVA procedures, featuring a 95% confidence interval and incorporating four key factors: Cell type (AD-MSC, NHDF), Materials (SF-Fr-D, SF-Fr-O, SF-Ft), Time (0, 4, 7, 11, 17, 23, 29, 38, 42, 48, 60, 72 h), and Concentration (85, 250, 450 μg/mL). The interaction plot assessed (b) material × hour interactions (c) cell × material interactions, and (d) concentration × material interactions. Tukey test was used for pairwise comparisons between the two groups, with statistical significance set at $p < 0.05$. The F-value assessed differences between group means.

considered. In the case of NHDFs CM, the combination of NHDF and SF-Ft resulted in superior wound closure. Conversely, AD-MSCs CM exhibited a more discerning response, with SF-Ft and SF-Fr-D positively affecting wound closure.

Concentration exerts a significant influence on CM's effectiveness (Supporting Information S1: Table S1). The obvious interactions observed between the material and concentration highlight that CM contains not only beneficial cytokines but also cellular metabolic byproducts. Hence, striking a balanced concentration is of importance (Figure 4d). At a low CM concentration (85 μg/mL), CM sourced from all materials exhibited similar levels of effectiveness, with no significant difference. However, as the concentration increased, noteworthy distinctions emerged in the performance of CM sourced from SF-Ft and SF-Fr-D in comparison to SF-Fr-O. SF-Ft sourced CM notably enhanced NHDFs migration, and this effect became more pronounced at higher CM concentrations (450 and 250 μg/mL). Particularly, at a concentration of 250 μg/mL, SF-Ft CM demonstrated optimal performance with a significant difference from SF-Fr-O CM.

In summary, SF topological structures can influence the secretion of cells, thereby affecting the chemotactic behavior of NHDFs and improving migration efficiency. Upon stimulation by fibrous and flat structures, cells secreted a greater quantity of factors related to cell migration. However, it cannot definitively conclude how precisely impacts cellular paracrine signaling. SF-Ft, distinguished by its smooth surface combined with SF, reduced cell anchoring points, resulting in enhanced cell viability. Furthermore, these findings support the notion that this SF surface can induce cells to secrete more migration-related factors. It is speculated that cells on aligned fibers undergo elongation and orientation changes in cell state, leading to the secretion of various other factors and potentially contributing to a slower migration speed. Considering the interaction effects between materials and cell types, a promising approach to address varying treatment requirements is the customization of cell selection along with the corresponding microenvironment they necessitate.

3.4 | Cell morphology on the SF materials

Figure 5 presents a comprehensive overview of AD-MSC behavior on various SF materials over the course of 1, 3, and 5 days. These AD-MSCs were fluorescently labeled with FDA to facilitate the visualization of live cells characterized by intact cell membranes (Figure 5a). The primary emphasis here lies in the assessment of cell orientation, a parameter significantly influenced by the cues

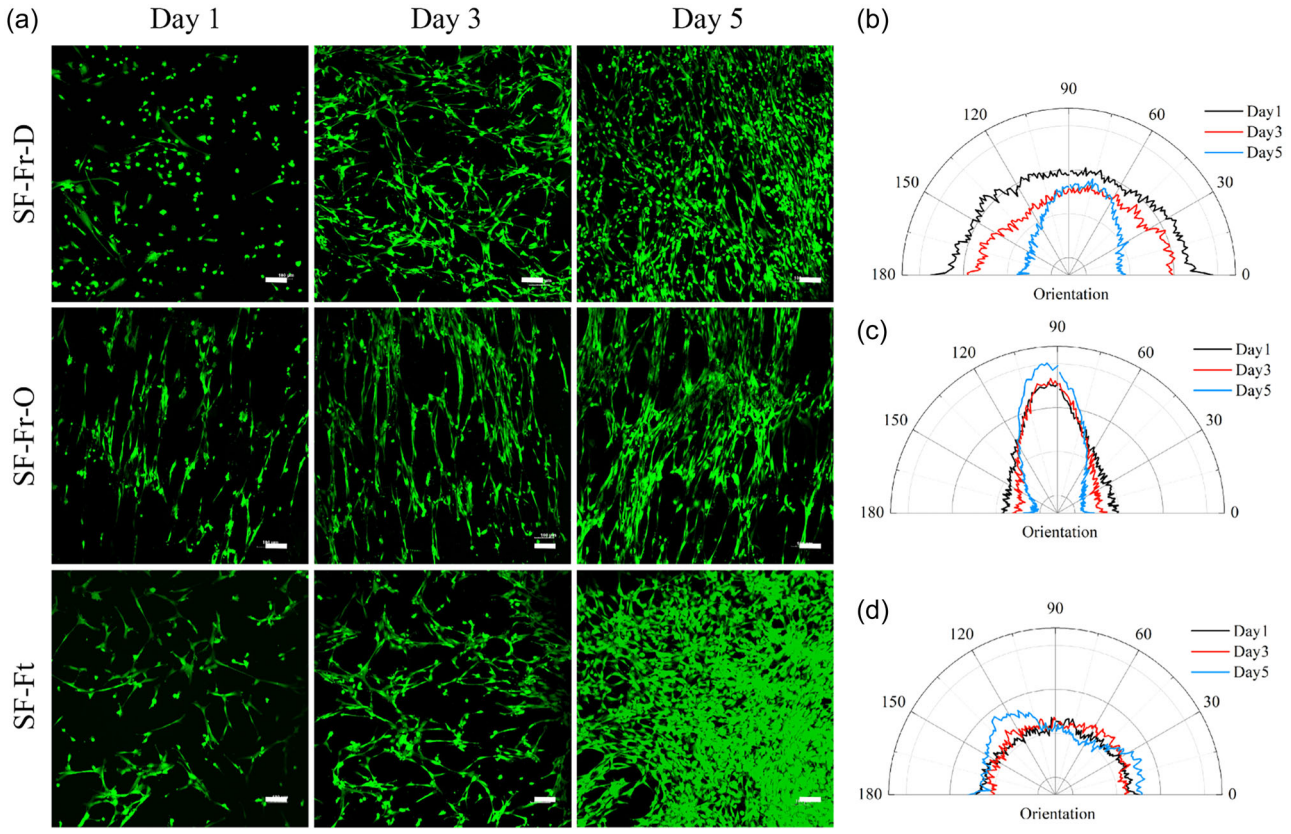

FIGURE 5 (a) Fluorescence images of adipose tissue-derived mesenchymal stem cells (AD-MSCs) from passage 8, cultured on SF-Fr-D, SF-Fr-O, and SF-Ft surfaces for 1, 3, and 5 days. These images were captured utilizing the fluorescein diacetate as a molecular probe to visualize the live cell morphology (in green). The summation of radial pixel intensity plots against the acquisition angle for cell morphology on various material surfaces was subjected to Fast Fourier Transform, which represents cell orientation. Cell orientation of AD-MSCs cultivated on (b) SF-Fr-D, (c) SF-Fr-O, and (d) SF-Ft for days 1, 3, and 5 is delineated in these plots. The scale bar in all images is 100 μm.

emanating from the material surface. Fluorescence images underwent FFT processing to evaluate AD-MSCs orientation, as portrayed in Figure 5b–d.

On day 1, AD-MSCs exhibited a spherical morphology and dispersed randomly on SF-Fr-D. Conversely, AD-MSCs cultured on SF-Fr-O and SF-Ft displayed a spindle-like shape. This phenomenon was substantiated by the orientation statistics presented in Figure 4b–d. The cell orientation curves for SF-Fr-D and SF-Ft appeared uniform, indicating isotropic and stochastic cell orientation. Notably, on SF-Fr-O, AD-MSCs displayed a high degree of alignment, extending along the fibers, as indicated by the narrow and nearly vertical cell orientation curve, approximating 90°.

By day 3, AD-MSC behavior closely mirrored that of day 1, accompanied by active cell proliferation and consistent cell orientation. However, by day 5, a noteworthy observation emerged: AD-MSCs consistently maintained a significantly aligned orientation on the SF-Fr-O surface, albeit with slower proliferation. In contrast, AD-MSCs were evenly distributed on the SF-Fr-D surface compared to days 1 and 3. On the surface of SF-Ft, AD-MSCs proliferated rapidly and formed multilayered cell structures in some areas. The results indicate that different material surface topologies have the capability to influence cell behaviors and aligned arrangement of fiber structures can effectively regulate the directional cell growth.

The behaviors of NHDFs on diverse surfaces closely mirrored those of AD-MSCs, with a specific focus on cell orientation. Fluorescence images of NHDFs from passage 10, cultivated on various SF materials, are depicted in Figure 6a. On day 1, NHDFs exhibited a spindle-shaped morphology and displayed anisotropic orientation on SF-Fr-D and SF-Ft (Figure 6b,d). The cell orientation curves for these surfaces were consistent, indicating that NHDFs grew and migrated without any notable directional bias. In contrast, NHDFs on the SF-Fr-O surface demonstrated a remarkable degree of orientation, corroborated by the narrow peak in the statistical data for cell orientation (Figure 6c). The conditions on day 3 remained akin to those on day 1, with the exception of heightened cell proliferation. By day 5, little disparity was observed among SF-Fr and SF-Fr-D, as NHDFs had covered the entire surface. Surprisingly, NHDFs on SF-Fr-O retained a high level of orientation from day 1 to day 5, even as proliferation continued. Nevertheless, as NHDFs proliferated on the SF-Fr-O surface, the level of orientation gradually declined, resulting in a broader peak in the statistical data.

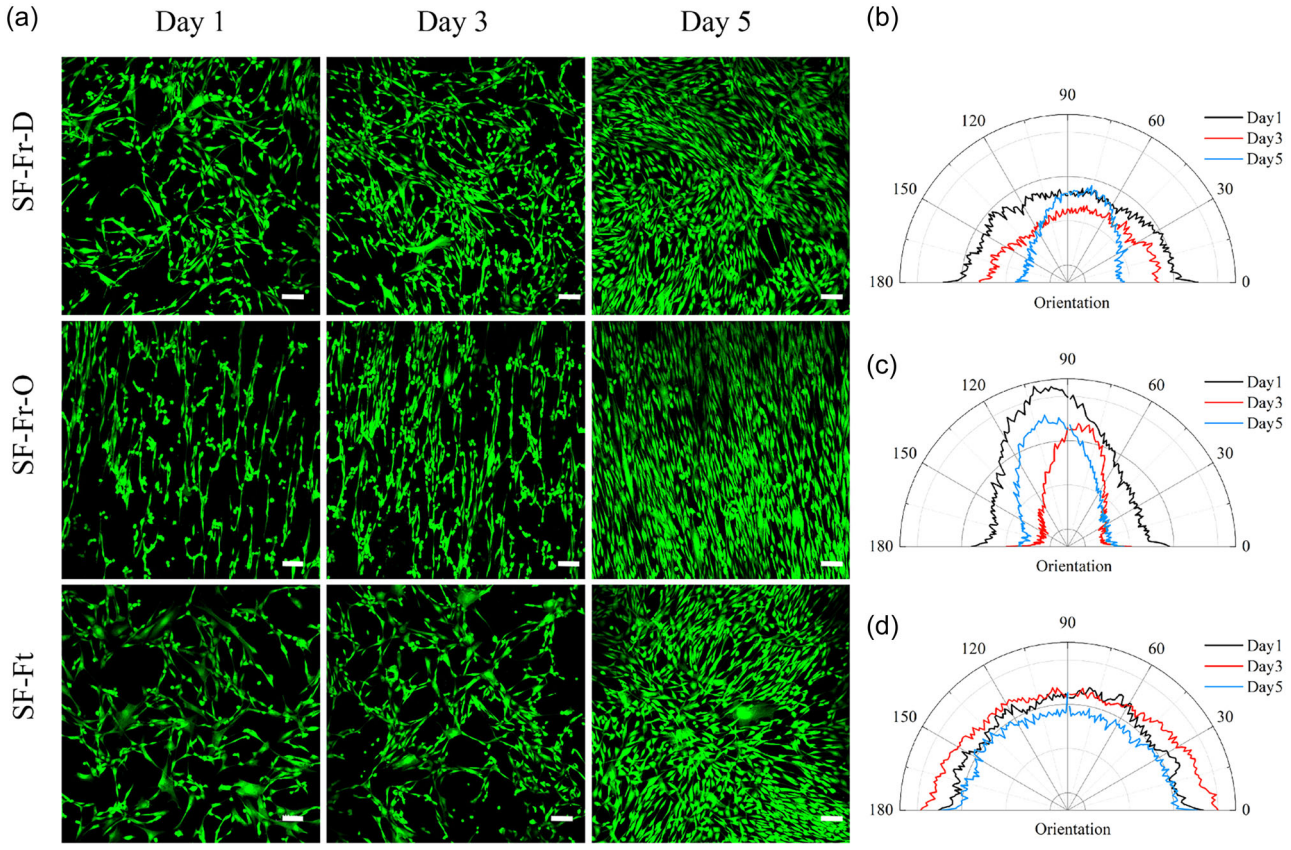

FIGURE 6 (a) Fluorescence images of normal human dermal fibroblasts from passage 10, cultured on SF-Fr-D, SF-Fr-O, and SF-Ft surfaces for 1, 3, and 5 days. These images were captured utilizing fluorescein diacetate as a molecular probe to visualize the live cell morphology (in green). The summation of radial pixel intensity plots against the acquisition angle for cell morphology on various material surfaces was subjected to Fast Fourier Transform, which represents cell orientation. Cell orientation of adipose tissue-derived mesenchymal stem cells cultivated on (b) SF-Fr-D, (c) SF-Fr-O, and (d) SF-Ft for days 1, 3, and 5 is delineated in these plots. The scale bar in all images is 100 μm.

In comparison to AD-MSCs, NHDFs exhibited analogous behaviors when cultivated on various SF materials. Cells on SF-Fr-D and SF-Ft displayed similar morphological characteristics, with cells growing isotopically. However, unlike AD-MSCs, NHDFs did not maintain robust alignment on the aligned fibrous membranes (SF-Fr-O), indicating a comparatively weaker influence of aligned fibers on NHDF orientation. Both cell types exhibited enhanced proliferation when cultured on SF materials in contrast to the control, and their morphological characteristics varied depending on the substrate. Notably, AD-MSCs on SF-Fr-O on day 5 continued to exhibit a high degree of orientation despite slower proliferation. This underscores the potential of SF materials to offer customizable microenvironments with significant topographical cues for modulating cell behavior (Li et al., 2021).

The SEM imaging of cell–substrate interactions provided further insight into the morphological changes of AD-MSCs and NHDFs on different material surfaces (Figure 7). These images supported the findings from fluorescence imaging and revealed distinct morphological characteristics of the two cell types. NHDFs were larger in size, approximately 50 µm, while AD-MSCs were smaller, around 20 µm. Furthermore, NHDFs exhibited a slender, spindle-like shape, whereas AD-MSCs had a rounder morphology. In comparison to SF-Ft, both AD-MSCs and NHDFs displayed more filopodia on the fibrous membranes (SF-Fr-D, SF-Fr-O). This phenomenon can be attributed to the higher surface-area-to-volume ratio of fibrous membranes, which provides additional anchoring sites for cell attachment (Dong et al., 2021). Notably, the filopodia of cells on SF-Fr-D extended in various directions, while on SF-Fr-O, they elongated along the fibers. This observation suggests that the fibrous membrane structure can guide the extension of cell skeletons, particularly in the case of AD-MSCs.

AD-MSCs exhibit a significantly larger spreading area on SF-Ft compared to the fibrous membrane (Figure 7b), but the fibers on the SF-Fr-O can maintain their elongation. The spreading area of NHDFs on both SF-Fr-D and SF-Fr-O increased to varying degrees (Figure 7d), with NHDFs on the SF-Fr-D showing greater elongation (Figure 7e). These results indicate that the topological microstructure of the substrate can significantly affect NHDFs spreading and their alignment.

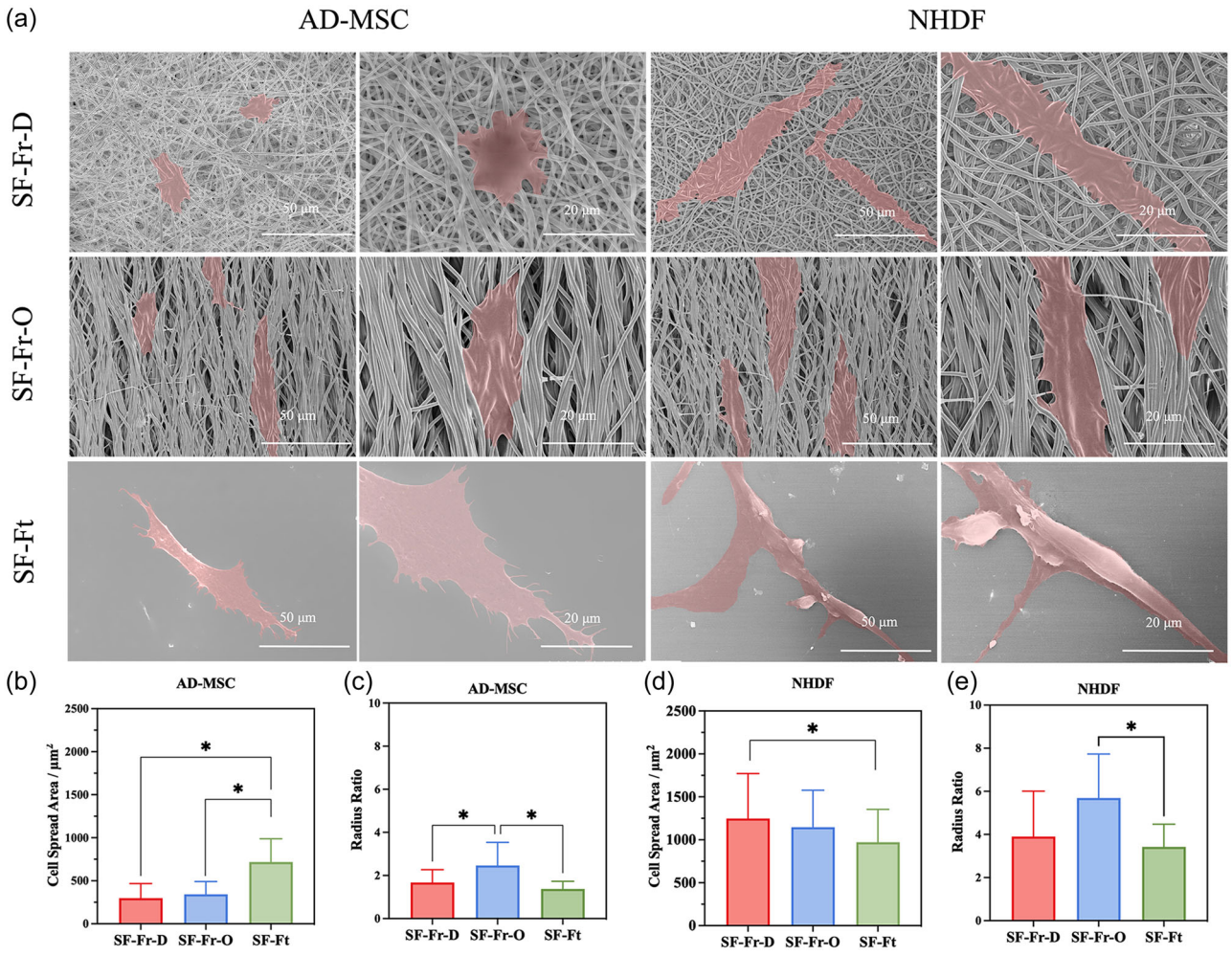

FIGURE 7 (a) Scanning electron microscope (SEM) images captured on day 3, showcasing the morphology of adipose tissue-derived mesenchymal stem cells (AD-MSCs) and normal human dermal fibroblasts (NHDFs) cultured on SF-Fr-D, SF-Fr-O, and SF-Ft. Quantification of (b) cell spread area and (c) radius ratio of AD-MSCs. Quantification of (d) cell spread area and (e) radius ratio of NHDFs. All values are presented as mean ± SEM. Statistical significance was determined using an unpaired two-tailed Student's *t*-test. $^*P < 0.01$.

3.5 | Physical cues for migration

The microenvironment not only influences cellular secretion but also directly impacts cell motility. Topographical structures effectively regulate cellular behaviors through physical cues that geometrically restrict adhesion sites, guiding directional migration (Wang et al., 2021). Aligned fibers, for instance, can mimic various natural soft tissues, actively guiding cell migration and orientation (Celie et al., 2019), ultimately contributing to the promotion of wound healing (He et al., 2022). In vitro cell motility monitoring assays can be used to evaluate the effect of material topology on cell orientation behavior and explore its possibility as a wound healing material. To gain a deeper understanding of NHDFs' migration on various material surfaces, an individual cell tracking-based strategy was employed. This approach allowed us to thoroughly analyze various aspects of cell migration. ImageJ plugin was utilized to track PKH-26 labeled membranes and record the locations of individual cells over a 24-h period (Videos S1–S3). Based on these tracks, various cell migration metrics were calculated, including Euclidean and accumulated distances, cell velocity, and mean cell directionality (Supporting Information S1: Figure S3 and Table S2). The Euclidean distance for each cell was determined as the length of the straight line between the cell's starting and ending points. The accumulated distance for each cell represented the sum of all incremental movements measured between individual images. Directionality, a metric that evaluates the extent to which a cell's movement aligns with a straight line and represents migration efficiency, was determined by dividing the Euclidean distance by the accumulated distance for each cell. Velocity was calculated as the mean value obtained by dividing the accumulated distance by the tracking time (24 h).

After analysis, it was found that fibers provide NHDFs with significant physical cues' guidance in direction, velocity, and migration efficiency, compared to the flat surfaces. NHDFs on SF-Fr-O and SF-Fr-D exhibit directed migration along the fiber direction, resulting in increasing directedness values during the 24-h tracking period (Figure 8a, Supporting Information S1: Table S2). While the velocity of NHDFs on SF-Fr-D and SF-Fr-O is 6.867 ± 0.2803 and 6.703 ± 0.3937 μm/min, which is nearly 2 times higher than that on SF-Ft (Figure 7b, Supporting Information S1: Table S2), respectively. Additionally, both the Euclidean distance and accumulated distance measurements support this observation (Figure 8c,d). The Euclidean distance covered by NHDFs on the SF-Fr-O surface is greater than that on SF-Fr-D, reflecting a more purposeful initial NHDFs migration that enables NHDFs to spread more rapidly and in a more defined manner. SF's cytophilic functional groups could enhance cell migration by modulating the interaction between cells and the SF material surface. The migration directedness of NHDFs on SF-Fr-O and SF-Fr-D reaches 0.6434 and 0.4349, respectively, indicating higher migration efficiency compared with the SF-Ft (Figure 8e). Fibers offer a greater number of adhesion sites and directional cues for cell movement, resulting in enhanced cell migration speed and directionality during each movement cycle. SF-Fr-D exhibits a disordered fiber arrangement, while SF-Fr-O features highly aligned fibers. Although NHDFs migrate along the fibers on both surfaces, the distinct surface morphologies of SF-Fr-O and SF-Fr-D lead to differences in cell movement direction. Specifically, NHDFs movement on SF-Fr-D appears more disorganized, whereas on SF-Fr-O, it is more purposeful, as indicated by the directionality value.

In summary, membranes with aligned fibers (SF-Fr-O) create an optimized microenvironment for NHDFs to migrate effectively. The results of this study highlight the important influence of material's structural factors, including fibrous topology and its orientation, to enhance cell migration speed and directedness. Compared with the flat and smooth SF membrane surface, the material surface with a fibrous structure can effectively promote the cell migration rate. In addition, regulating the spatial aligned arrangement of fiber structures can significantly expand the spatial range of cell movement, especially the cell migration distance in specific directions. These findings may provide insights into designing novel wound healing materials for precision treatment in wound healing therapies.

4 | CONCLUSION

In this investigation, an array electrospinning collector was innovatively designed to fabricate the electrospun patterned SF membrane comprising both aligned and randomly arranged SF fibers. This unique electrospinning process allowed precise control over the orientation distribution of SF fibers through electrostatic manipulation, resulting in the integration of both aligned and random fiber layers. Additionally, the size of the fibrous membrane was expanded by configuring the electrospinning collector arrangement and improving the mechanical properties of the aligned membrane. The resulting membrane showcased an alternating patterned structure, featuring regions with both disordered and ordered fiber distributions. This configuration generated a large-area membrane with outstanding stability, prompting further exploration into the influence of SF fiber membrane topology on cell behaviors and its potential applications as a material for wound repair. Conducting in vitro cell toxicity assays using AD-MSCs and NHDFs cells demonstrated that the prepared SF fiber membranes exhibited no significant toxic effects, indicating commendable biocompatibility. Furthermore, the investigation delved into understanding the specific microenvironments that could influence the formulation of cells' CM, consequently enhancing wound healing efficiency. CMs derived from both AD-MSCs and NHDFs when cultured on SF-Ft exhibited the ability to promote cell migration. Notably, CMs from AD-MSCs showcased a substantial increase in protein concentration when cultured on SF-Fr-O. Moreover, the topography of electrospun SF materials significantly influenced cell behavior, impacting cell morphology, migration velocity, and chemotaxis. Membranes composed of aligned fibers (SF-Fr-O) created an optimized microenvironment that facilitated effective NHDF migration. This effect suggested that these fibers provided enhanced adhesion sites and directional cues, leading to accelerated cell migration speed and improved directionality.

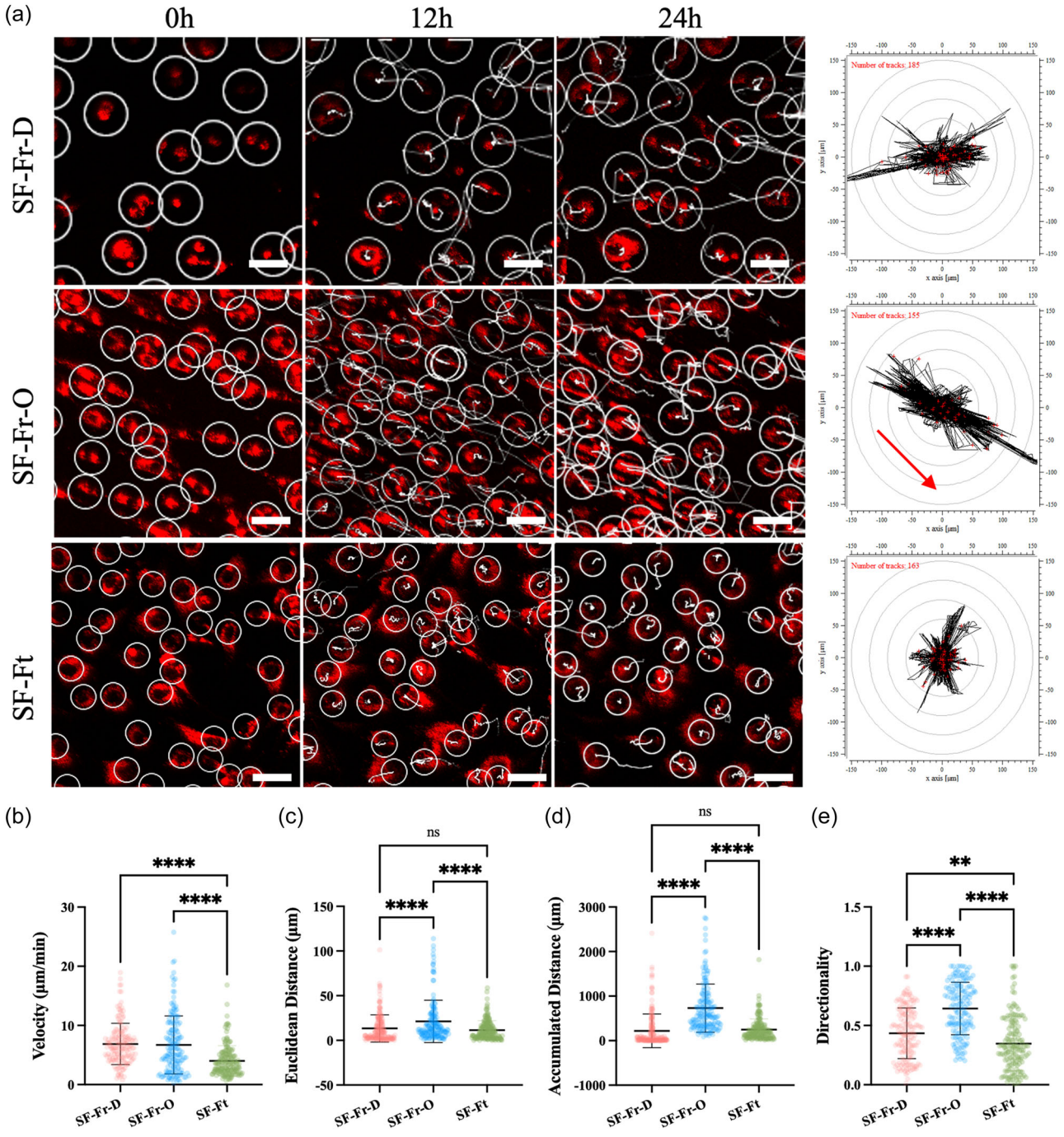

FIGURE 8 Tracking of normal human dermal fibroblasts (NHDFs) migratory behaviors on SF-Fr-D, SF-Fr-O, and SF-Ft over 24 h at 30-min intervals. (a) Fluorescence images of the observation area, where NHDFs labeled with PKH26 are shown in red. Trajectory plots were generated based on the tracking of NHDFs from the selected area, illustrating the vectors each cell has moved from the origin. Additionally, all tracks were adjusted to share a common origin (the intersection of the *x* and *y* axes) using the Chemotaxis plugin of ImageJ, and the red cross represents the end point of the trajectory: SF-Fr-D, SF-Fr-O, and SF-Ft. The red arrow indicates the direction of the fibers. Trajectories for each condition were quantified from the track plot of three independent experiments, measuring: (b) velocity, (c) Euclidean distance, (d) accumulated distance, and (e) directionality of migration. Accumulated distance refers to the sum of all cell paths, while the Euclidian distance represents the length of a straight line between the cell's start and end points, as observed in the trajectory plots. Directionality is calculated by comparing the Euclidian distance to the accumulated distance, providing insight into the straightness of migration. Each symbol represents an individual cell, and the data were collected from three independent experiments. All values are presented as mean ± scanning electron microscope. Statistical significance was determined using an unpaired two-tailed Student's *t*-test. $^{**}p < 0.01$, $^{***}p < 0.001$, $^{****}p < 0.0001$. Scale bar = 50 μm.

Conclusively, the investigation highlighted the potential of tuning the microenvironment to tailor secretion productions and material topography cues for guiding directional cell migration, offering promising avenues for augmenting wound healing efficiency.

AUTHOR CONTRIBUTIONS

Hua Ye, Ke-Qin Zhang, and Hui Wang contributed to the initial conceptual and experimental design. Jia-Chen Zhu conducted the fabrication of SF materials experiments with assistance from Chen-Xing Wu. Chen-Xing Wu conducted the mechanical properties experiment. Jia-Chen Zhu performed other experiments and data analysis under the supervision of Hua Ye, Ke-Qin Zhang, and Hui Wang. Jia-Chen Zhu prepared the initial draft of the manuscript, which was then revised by Hua Ye, Ke-Qin Zhang, and Hui Wang. All authors approved the final manuscript.

ACKNOWLEDGMENTS

This work was supported by joint Projects of International Exchanges between National Natural Science Foundnation of China (51911530207) and Royal Society (IEC\NSFC\181408), Natural Science Foundation of Jiangsu Province of China (BK20211317), China National Textile and Apparel Council Key Laboratory for Silk Functional Materials and Technology, and Priority Academic Program Development of Jiangsu Higher Education Institutions.

DATA AVAILABILITY STATEMENT

The data sets used and analyzed during the current study are available from the corresponding author on reasonable request.

ORCID

Jia-Chen Zhu http://orcid.org/0009-0005-3557-0008
Hui Wang http://orcid.org/0000-0002-4496-2418
Ke-Qin Zhang http://orcid.org/0000-0002-7615-6509
Hua Ye http://orcid.org/0000-0001-7613-6041

REFERENCES

Brandley, E., Greenhalgh, E. S., Shaffer, M. S. P., & Li, Q. (2018). Mapping carbon nanotube orientation by fast Fourier transform of scanning electron micrographs. *Carbon*, *137*, 78–87. https://doi.org/10.1016/j.carbon.2018.04.063

Celie, K. B., Toyoda, Y., Dong, X., Morrison, K. A., Zhang, P., Asanbe, O., Jin, J. L., Hooper, R. C., Zanotelli, M. R., Kaymakcalan, O., Bender, R. J., & Spector, J. A. (2019 June). Microstructured hydrogel scaffolds containing differential density interfaces promote rapid cellular invasion and vascularization. *Acta Biomaterialia*, *91*, 144–158. https://doi.org/10.1016/j.actbio.2019.04.027

Collins, M. N., Ren, G., Young, K., Pina, S., Reis, R. L., & Oliveira, J. M. (2021). Scaffold fabrication technologies and structure/function properties in bone tissue engineering. *Advanced Functional Materials*, *31*(21). https://doi.org/10.1002/adfm.202010609

Dahbour, S., Jamali, F., Alhattab, D., Al-Radaideh, A., Ababneh, O., Al-Ryalat, N., Al-Bdour, M., Hourani, B., Msallam, M., Rasheed, M., Huneiti, A., Bahou, Y., Tarawneh, E., & Awidi, A. (2017). Mesenchymal stem cells and conditioned media in the treatment of multiple sclerosis patients: Clinical, ophthalmological and radiological assessments of safety and efficacy. *CNS Neuroscience & Therapeutics*, *23*(11), 866–874. https://doi.org/10.1111/cns.12759

Dong, Z., Meng, X., Yang, W., Zhang, J., Sun, P., Zhang, H., Fang, X., Wang, D. A., & Fan, C. (2021 March). Progress of gelatin-based microspheres (GMSs) as delivery vehicles of drug and cell. *Materials Science and Engineering: C*, *122*, Article 111949. https://doi.org/10.1016/j.msec.2021.111949

Gao, C., Zhang, L., Wang, J., Jin, M., Tang, Q., Chen, Z., Cheng, Y., Yang, R., & Zhao, G. (2021 April 14). Electrospun nanofibers promote wound healing: Theories, techniques, and perspectives. *Journal of Materials Chemistry B*, *9*(14), 3106–3130. https://doi.org/10.1039/d1tb00067e

Ge, Y., Miao, Y., Gur-Cohen, S., Gomez, N., Yang, H., Nikolova, M., Polak, L., Hu, Y., Verma, A., Elemento, O., Krueger, J. G., & Fuchs, E. (2020 March 10). The aging skin microenvironment dictates stem cell behavior. *Proceedings of the National Academy of Sciences*, *117*(10), 5339–5350. https://doi.org/10.1073/pnas.1901720117

Gholipourmalekabadi, M., Sapru, S., Samadikuchaksaraei, A., Reis, R. L., Kaplan, D. L., & Kundu, S. C. (2020 January 1). Silk fibroin for skin injury repair: Where do things stand. *Advanced Drug Delivery Reviews*, *153*, 28–53. https://doi.org/10.1016/j.addr.2019.09.003

He, C., Yu, B., Lv, Y., Huang, Y., Guo, J., Li, L., Chen, M., Zheng, Y., Liu, M., Guo, S., Shi, X., & Yang, J. (2022). Biomimetic asymmetric composite dressing by electrospinning with aligned nanofibrous and micropatterned structures for severe burn wound healing. *ACS Applied Materials & Interfaces*, *14*(29), 32799–32812. https://doi.org/10.1021/acsami.2c04323

Huang, G., Li, F., Zhao, X., Ma, Y., Li, Y., Lin, M., Jin, G., Lu, T. J., Genin, G. M., & Xu, F. (2017 October 25). Functional and biomimetic materials for engineering of the three-dimensional cell microenvironment. *Chemical Reviews*, *117*(20), 12764–12850. https://doi.org/10.1021/acs.chemrev.7b00094

Imaichi-Kobayashi, S., Kassab, R., Piersigilli, A., Robertson, R., Leonard, C., Long, N., Dean, B., Phaneuf, M., & Ling, V. (2023). An electrospun macrodevice for durable encapsulation of human cells with consistent secretion of therapeutic antibodies. *Biomaterials*, *298*, Article 122123. https://doi.org/10.1016/j.biomaterials.2023.122123

In Kim, J., & Kim, C. S. (2018 October 1). Harnessing nanotopography of PCL/collagen nanocomposite membrane and changes in cell morphology coordinated with wound healing activity. *Materials Science and Engineering: C*, *91*, 824–837. https://doi.org/10.1016/j.msec.2018.06.021

Ji, X., Li, R., Jia, W., Liu, G., Luo, Y., & Cheng, Z. (2020). Co-axial fibers with Janus-structured sheaths by electrospinning release corn peptides for wound healing. *ACS Applied Bio Materials*, *3*(9), 6430–6438. https://doi.org/10.1021/acsabm.0c00860

Jiao, F., Zhao, W., Zhao, W., Wang, Y., Deng, Y., Chang, S., Sun, J., Lou, Q., Wang, L., Shan, C. X., Xiao, Y., & Dong, L. (2023). Biomass-derived washable composites for accelerating the healing of infected wounds. *BMEMat*, *1*(4). https://doi.org/10.1002/bmm2.12055

Kadir, N. D., Yang, Z., Hassan, A., Denslin, V., & Lee, E. H. (2021 February 3). Electrospun fibers enhanced the paracrine signaling of mesenchymal stem cells for cartilage regeneration. *Stem Cell Research & Therapy*, *12*(1), Article 100. https://doi.org/10.1186/s13287-021-02137-8

Kadunc Polajnar, L., Lainšček, D., Gašperšič, R., Sušjan-Leite, P., Kovačič, U., Butinar, M., Turk, B., Jerala, R., & Hafner-Bratkovič, I. (2023). Engineered combinatorial cell device for wound healing and bone regeneration. *Frontiers in Bioengineering and Biotechnology*, *11*, Article 1168330. https://doi.org/10.3389/fbioe.2023.1168330

Li, J., Liu, Y., Zhang, Y., Yao, B., Enhejirigala, Li, Z., Song, W., Wang, Y., Duan, X., Yuan, X., Fu, X., & Huang, S. (2021). Biophysical and biochemical cues of biomaterials guide mesenchymal stem cell behaviors. *Frontiers in Cell and Developmental Biology*, *9*, Article 640388. https://doi.org/10.3389/fcell.2021.640388

Li, Y., Xiao, Y., & Liu, C. (2017 March 8). The horizon of materiobiology: A perspective on material-guided cell behaviors and tissue engineering. *Chemical Reviews*, *117*(5), 4376–4421. https://doi.org/10.1021/acs.chemrev.6b00654

Lian, M., Sun, B., Han, Y., Yu, B., Xin, W., Xu, R., Ni, B., Jiang, W., Hao, Y., Zhang, X., Shen, Y., Qiao, Z., & Dai, K. (2021 July). A low-temperature-printed hierarchical porous sponge-like scaffold that promotes cell-material interaction and modulates paracrine activity of MSCs for vascularized bone regeneration. *Biomaterials*, *274*, Article 120841. https://doi.org/10.1016/j.biomaterials.2021.120841

Loesel, K. E., Hiraki, H. L., Baker, B. M., & Parent, C. A. (2023). An adaptive and versatile method to quantitate and characterize collective cell migration behaviors on complex surfaces. *Frontiers in Cell and Developmental Biology*, *11*, Article 1106653. https://doi.org/10.3389/fcell.2023.1106653

Maarof, M., Lokanathan, Y., Ruszymah, H. I., Saim, A., & Chowdhury, S. R. (2018). Proteomic analysis of human dermal fibroblast conditioned medium (DFCM). *The Protein Journal*, *37*(6), 589–607. https://doi.org/10.1007/s10930-018-9800-z

Memic, A., Abdullah, T., Mohammed, H. S., Joshi Navare, K., Colombani, T., & Bencherif, S. A. (2019 March 18). Latest progress in electrospun nanofibers for wound healing applications. *ACS Applied Bio Materials*, *2*(3), 952–969. https://doi.org/10.1021/acsabm.8b00637

Mousavi, S. M., Nejad, Z. M., Hashemi, S. A., Salari, M., Gholami, A., Ramakrishna, S., Chiang, W. H., & Lai, C. W. (2021 September 13). Bioactive agent-loaded electrospun nanofiber membranes for accelerating healing process: A review. *Membranes*, *11*(9). https://doi.org/10.3390/membranes11090702

Navaneethan, B., Vijayakumar, G. P., Ashang Luwang, L., Karuppiah, S., Jayarama Reddy, V., Ramakrishna, S., & Chou, C.-F. (2021). Novel self-directing single-polymer jet developing layered-like 3D buckled microfibrous scaffolds for tissue engineering applications. *ACS Applied Materials & Interfaces*, *13*(8), 9691–9701. https://doi.org/10.1021/acsami.0c22028

Nogueira, G. M., Rodas, A. C. D., Leite, C. A. P., Giles, C., Higa, O. Z., Polakiewicz, B., & Beppu, M. M. (2010 November). Preparation and characterization of ethanol-treated silk fibroin dense membranes for biomaterials application using waste silk fibers as raw material. *Bioresource Technology*, *101*(21), 8446–8451. https://doi.org/10.1016/j.biortech.2010.06.064

Oroujzadeh, M., Mosaffa, E., & Mehdipour-Ataei, S. (2024). Recent developments on preparation of aligned electrospun fibers: Prospects for tissue engineering and tissue replacement. *Surfaces and Interfaces*, *49*. https://doi.org/10.1016/j.surfin.2024.104386

Tindell, R. K., Busselle, L. P., & Holloway, J. L. (2023). Magnetic fields enable precise spatial control over electrospun fiber alignment for fabricating complex gradient materials. *Journal of Biomedical Materials Research. Part A*, *111*(6), 778–789.

Robinson, A. J., Pérez-Nava, A., Ali, S. C., González-Campos, J. B., Holloway, J. L., & Cosgriff-Hernandez, E. M. (2021 March 3). Comparative analysis of fiber alignment methods in electrospinning. *Matter*, *4*(3), 821–844. https://doi.org/10.1016/j.matt.2020.12.022

Sharifi, S., Hajipour, M. J., Gould, L., & Mahmoudi, M. (2020). Nanomedicine in healing chronic wounds: Opportunities and challenges. *Molecular Pharmaceutics*, *18*(2), 550–575. https://doi.org/10.1021/acs.molpharmaceut.0c00346

Shellard, A., & Mayor, R. (2020 November). All roads lead to directional cell migration. *Trends in Cell Biology*, *30*(11), 852–868. https://doi.org/10.1016/j.tcb.2020.08.002

Taylor, S. E, Cao, T., Talauliker, P. M., & Lifshitz, J. (2013). Objective morphological quantification of microscopic images using a fast Fourier transform (FFT) analysis. *Current Protocols Essential Laboratory Techniques*, *95*(Suppl 7), 9.5.1–9.5.12. https://doi.org/10.1002/9780470089941.et0905s07

Wang, L., Mao, L., Qi, F., Li, X., Wajid Ullah, M., Zhao, M., Shi, Z., & Yang, G. (2021). Synergistic effect of highly aligned bacterial cellulose/gelatin membranes and electrical stimulation on directional cell migration for accelerated wound healing. *Chemical Engineering Journal*, *424*. https://doi.org/10.1016/j.cej.2021.130563

Wang, S., Wu, W. Y., Yeo, J. C. C., Soo, X. Y. D., Thitsartarn, W., Liu, S., Tan, B. H., Suwardi, A., Li, Z., Zhu, Q., & Loh, X. J. (2023). Responsive hydrogel dressings for intelligent wound management. *BMEMat*, *1*(2). https://doi.org/10.1002/bmm2.12021

Xia, P., Wang, X., Qu, Y., Lin, Q., Cheng, K., Gao, M., Ren, S., Zhang, T., & Li, X. (2017 December 13). TGF-β1-induced chondrogenesis of bone marrow mesenchymal stem cells is promoted by low-intensity pulsed ultrasound through the integrin-mTOR signaling pathway. *Stem Cell Research & Therapy*, *8*(1), Article 281. https://doi.org/10.1186/s13287-017-0733-9

Xie, J., Wu, X., Zheng, S., Lin, K., & Su, J. (2022 July 26). Aligned electrospun poly(l-lactide) nanofibers facilitate wound healing by inhibiting macrophage M1 polarization via the JAK-STAT and NF-κB pathways. *Journal of Nanobiotechnology*, *20*(1), Article 342. https://doi.org/10.1186/s12951-022-01549-9

Yao, Q., Xue, Q., Li, Z., Zhang, K., Zhang, T., Li, N., Yang, S., Brabec, C. J., Yip, H. L., & Cao, Y. (2020). Graded 2D/3D perovskite heterostructure for efficient and operationally stable MA-free Perovskite solar cells. *Advanced Materials*, *32*(26). https://doi.org/10.1002/adma.202000571

Zhang, J., Liu, H., Yu, Q., Zhan, Z., Li, T., Shu, L., Zhang, C., Cheng, H., Zhang, T., Xin, H., & Wang, X. (2023). Hair derived microneedle patches for both diabetic foot ulcer prevention and healing. *ACS Biomaterials Science & Engineering*, *9*(1), 363–374. https://doi.org/10.1021/acsbiomaterials.2c01333

Zhang, Y., Luo, J., Zhang, Q., & Deng, T. (2021 December 15). Growth factors, as biological macromolecules in bioactivity enhancing of electrospun wound dressings for diabetic wound healing: A review. *International Journal of Biological Macromolecules*, *193*(Pt A), 205–218. https://doi.org/10.1016/j.ijbiomac.2021.09.210

SUPPORTING INFORMATION

Additional supporting information can be found online in the Supporting Information section at the end of this article.

How to cite this article: Zhu, J.-C., Wang, H., Wu, C.-X., Zhang, K.-Q., & Ye, H. (2024). Tailoring silk fibroin fibrous architecture by a high-yield electrospinning method for fast wound healing possibilities. *Biotechnology and Bioengineering*, 1–15. https://doi.org/10.1002/bit.28783